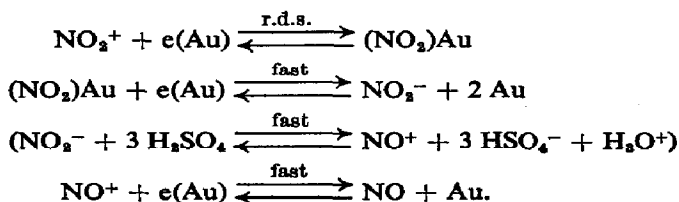


KINETICS AND MECHANISM OF THE ELECTRO-CHEMICAL REDUCTION OF NO_2^+ IN CONCENTRATED SULPHURIC ACID*

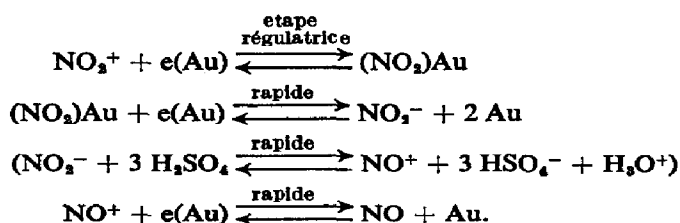
A. J. CALANDRA, C. TAMAYO, J. HERRERA and A. J. ARVÍA

Instituto de Investigaciones Fisicoquímicas Teóricas y Aplicadas, División Electroquímica, Facultad de Ciencias Exactas, Universidad Nacional de La Plata, La Plata, Argentina

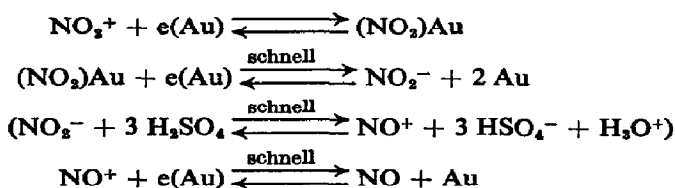
Abstract—The electrochemical reduction on gold of NO_2^+ dissolved in concentrated H_2SO_4 has been studied by means of the rotating disk electrode and cyclic voltammetry, over a wide range of experimental conditions. The kinetic parameters are interpreted in terms of the following reaction mechanism,



Résumé—Etude par voltamétrie cyclique, dans un domaine étendu de conditions expérimentales, de la réduction électrochimique sur électrodes d'or à disque tournant de NO_2^+ dissous dans H_2SO_4 concentré. Les paramètres cinétiques sont interprétés au moyen du mécanisme réactionnel:



Zusammenfassung—Man untersuchte die elektrochemische Reduktion von NO_2^+ , welches in konz. H_2SO_4 aufgelöst war. Die Untersuchungen erfolgten an einer rotierenden Scheibenelektrode aus Gold mit Hilfe zyklischer Voltametrie, wobei die experimentellen Bedingungen in einem weiten Bereich variiert wurden. Die Interpretation der kinetischen Parameter erfolgte unter der Annahme des folgenden Reaktionsmechanismus:



INTRODUCTION

ELECTROCHEMICAL studies on nitronium (nitryl) ion, NO_2^+ , are scarce. Masek^{1,2} studied this ion dissolved in sulphuric acid by polarography and later Topol, Osteryoung and Christie³ investigated its electrochemical behaviour by linear sweep voltammetry and chronopotentiometry using platinum and gold electrodes. There is

* Manuscript received 1 December 1971.

some qualitative agreement about the results of these authors. Thus, it was definitely established that NO^+ is formed as a consequence of the NO_2^+ reduction, independently of the metal used as electrode. But no quantitative kinetic data of possible independent reactions were available, although at least two possible reaction mechanisms were advanced.

In an attempt to obtain reliable quantitative data, we considered two definite aims (i) to establish a suitable electrode material yielding easily reproducible surfaces in the potential range where the electrode reaction are expected to occur and (ii) to study the NO^+/NO couple as a single reaction.

Concerning the first point we concluded that gold electrodes were suitable, if they were used fresh for each run. Platinum was discarded because oxide films are interfering at the potentials where NO_2^+ and NO^+ are reduced. Mercury is not suitable for the experimental techniques chosen, *viz* cyclic voltammetry and the rotating disk electrode.

The NO^+/NO couple behaves as a reversible electrode on gold in concentrated sulphuric acid, as recently reported.⁴ The over-all process does not involve NO_2^+ ; on the contrary, NO^+ is formed in the reduction of NO_2^+ . Thus, a first separation of the complex electrochemical process is achieved,⁴ which opens the possibility of establishing the more likely electrochemical reaction mechanism for the oxidation and reduction of NO_2^+ .

EXPERIMENTAL TECHNIQUE

The electrolysis cell was as previously described.⁴ The working electrode consisted of a mirror-polished gold disk electrode mounted in a Teflon rod. The geometrical area was 0.114 cm^2 . The electrode was cleaned before each run to achieve good reproducibility. It was noticed that when its surface was not freshly polished, the electrochemical behaviour corresponded to that of a more sluggish process (E/I cathodic curves were more "irreversible" and E/I voltograms slightly distorted as if the reaction resistance was increased).

A $\text{Hg}/\text{Hg}_2\text{SO}_4/\text{concentrated } \text{H}_2\text{SO}_4$ reference electrode was used. The reproducibility and stability of this electrode has been proved.⁵ The rest potential, E_r , of the clean working electrode was between 0.68 and 0.84 V, but when its surface was affected by some impurity E_r was about 0.38 V. The counter-electrode, as described before,⁴ was a platinum sheet of about 6 cm^2 kept in a separate compartment.

The NO_2^+ solutions were prepared from C. Erba reagent-grade NaNO_3 previously desiccated and C. Erba reagent-grade H_2SO_4 (96–98%), which were used without further purification. NO_2^+ is formed quantitatively⁶ by dissolution of NaNO_3 in H_2SO_4 .

The E/I curves were obtained with the potential-sweep apparatus described elsewhere,⁷ having compensation for the ohmic polarization. E/I curves with the electrode under rotation were recorded at 1 mV/s , approaching the conditions of quasi-stationary polarization curves. The rotation speed was varied from 283 to 2490 rev/min. Potential-sweep rates, v , from 5 to $5 \times 10^4 \text{ mV/s}$ were applied within a potential amplitude of 0.900 V, starting from the initial potential $E_1 = 0.800 \text{ V}$ towards the cathodic region. Potential-sweep voltograms were obtained either with the solution at rest or under stirring. Experiments involving only one voltammetric cycle as well as repetitive cycles were made. The NO_2^+ concentration was varied between 5.4 mM up to 56.5 mM. Runs were made from 5 to 56°C . Further experimental details have been given in previous publications.^{4,7}

RESULTS

Rotating disk electrode

Figure 1 contains typical cathodic E/I displays obtained with gold rotating disk electrodes at different concentrations. They exhibit two well defined current plateaux

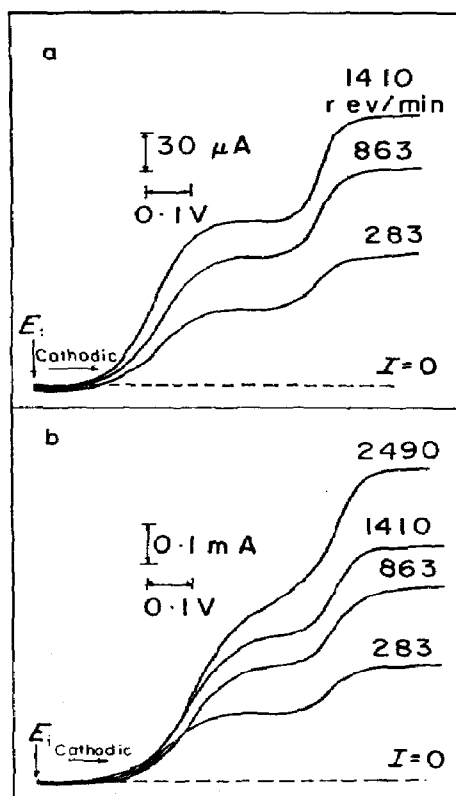


FIG. 1. Cathodic E/I curves at different rotation speeds of the gold rotating disk electrode.

a, c_0 , 9.2 mM; 15.5°C; v , 1 mV/s. b, c_0 , 28.8 mM; 15.5°C; v , 1 mV/s.

$(I_L)_I$ and $(I_L)_{II}$, the first between 0.4 and 0.6 V and the second at 0.8 V, the potentials being referred to the initial potential, E_1 .

The first current plateau varies linearly both with the square root of the rotation speed, ω and with NaNO_3 concentration, c_0 , as shown in Figs. 2 and 3. The second current plateau follows the same dependence as the first plateau both with ω and c_0 (Figs. 4 and 5). The current for the second plateau was measured taking as baseline the first current plateau. The total current read from the second plateau fits a relationship of the same type with ω and c_0 as the current of the individual plateaux (Figs. 6 and 7).

The cathodic E/I curves give linear $(E - E_1)$ vs $\log [(I_L - I)/I]$ plots (Fig. 8) with slope $2.3(2RT/F)$ for each curve. Although a particular E/I curve satisfied this slope, the reproducibility, with respect to the average line shown in Fig. 8, was not better than 25 mV. This figure gives also an idea of the reproducibility of the initial potential.

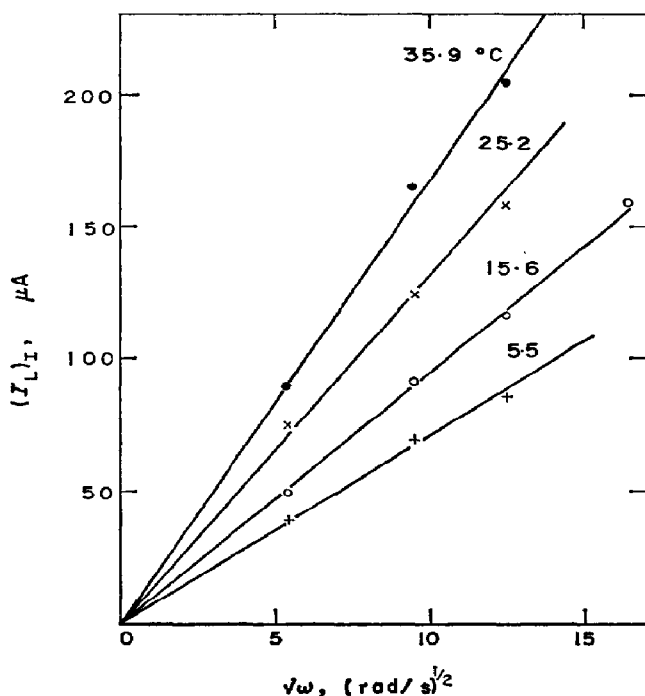


FIG. 2. Dependence of the first cathodic limiting current on the square root of the rotation speed: runs at different temperatures.
 c_0 , 9.2 mM.

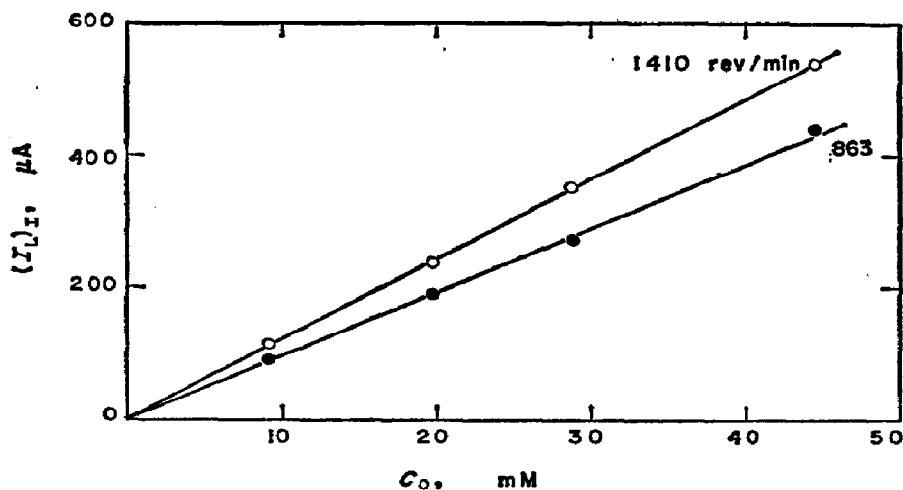


FIG. 3. Dependence of the first cathodic limiting current on NaNO_2 concentration.
 Runs at two different rotation speeds. 15°C.

The linear $(I_L)_I$ vs $\omega^{1/2}$ plot indicates a region where the process is under a convective-diffusion control. Therefore, by means of Newman's rotating-disk-electrode equation, the experimental diffusion coefficient of the reacting species was evaluated at the different temperatures.

To calculate the diffusion coefficient of the species related to the first current plateau, its concentration was taken as equal to c_0 and the number of electrons per particle as 2.

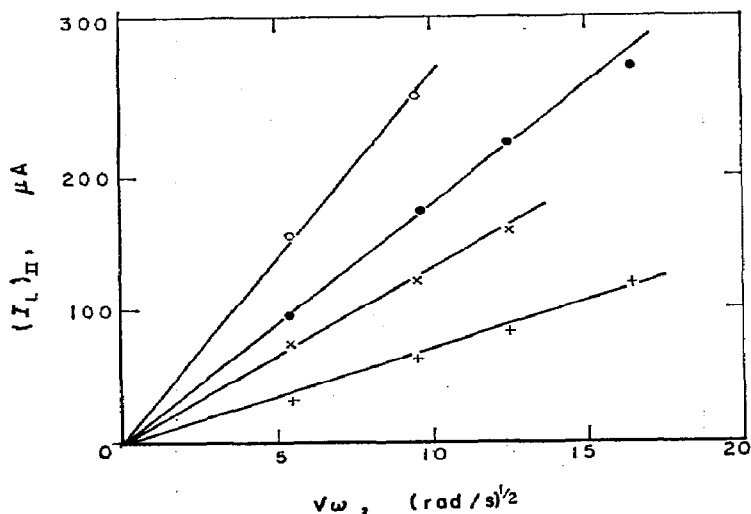


FIG. 4. Dependence of the second cathodic limiting current on the square root of the rotation speed. Runs at different temperatures and NaNO_2 concentrations. +, 5.04 mM, 25.5°C; ×, 19.9 mM, 15.1°C; ●, 28.8 mM, 15.5°C; ○, 44.5 mM, 15°C.

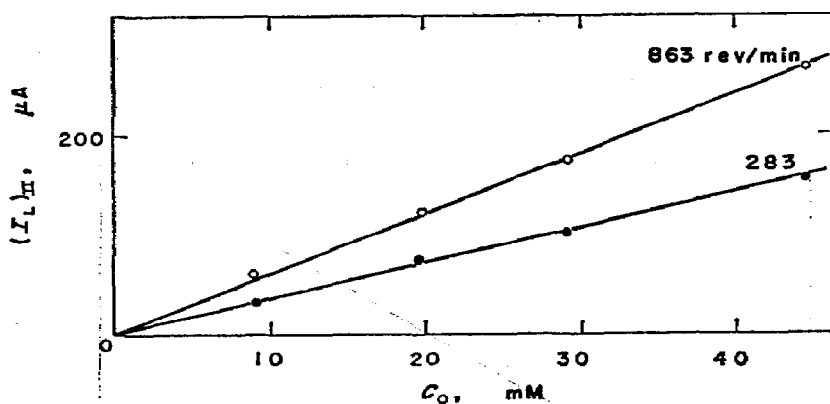


FIG. 5. Dependence of the second cathodic limiting current on NaNO_2 concentration. Runs at two different rotation speeds. 15°C.

Results are shown in the Arrhenius plot of Fig. 9. The slope of the straight line corresponds to an experimental activation energy of 5.98 ± 0.4 kcal/mole.

If the initial part of the E/I curve covering a ΔE region of about 0.3 V is plotted according to a Tafel equation, a straight line results as shown in Fig. 10 for different concentrations and rotation speeds, with a slope of $2.3(2RT/F)$. The same result was obtained by applying the treatment for processes under intermediate kinetics to a set of E/I curves obtained at different rotation speeds and starting from a reproducible E_1 value.

The half-wave potential of the first reaction is difficult to evaluate because the initial electrode potential is poorly reproducible and the same applies to the whole curve during the course of the first reaction. The E/I curve for the second reaction,

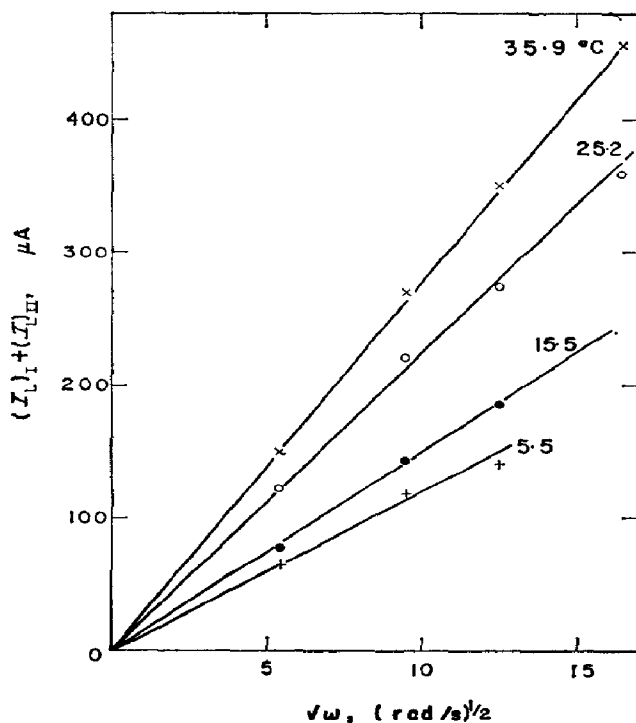


FIG. 6. Dependence of the total second current plateau on the square root of the rotation speed. Runs at different temperatures.
 c_0 , 0.2 mM.

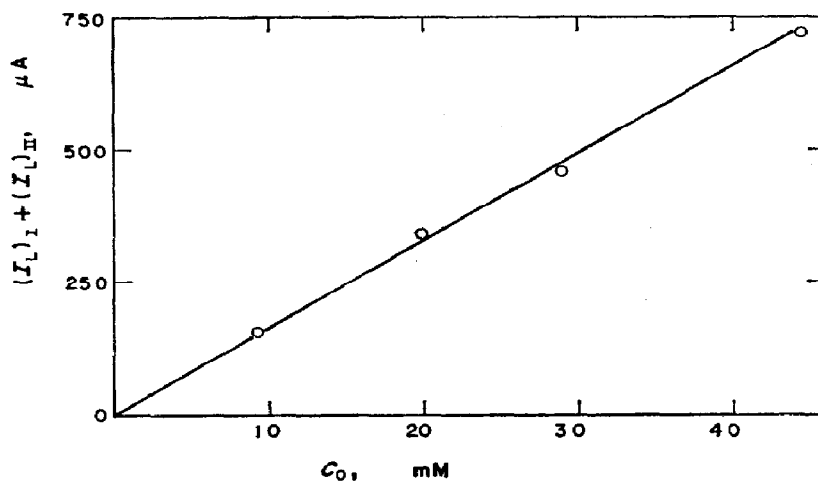


FIG. 7. Dependence of the total second current plateau on NaNO_2 concentration.
 $\omega = 100 \text{ rad/s}$; 15.5°C .

however, is more reproducible than the first, and its features are those already described for the NO/NO^+ electrode in concentrated sulphuric acid.⁴

Cyclic voltammetry

E/I voltagrams obtained with the solution at rest, at potential-sweep rates, v , from 25 mV/s to 7 V/s, covering a potential amplitude of about 0.9 V from the initial

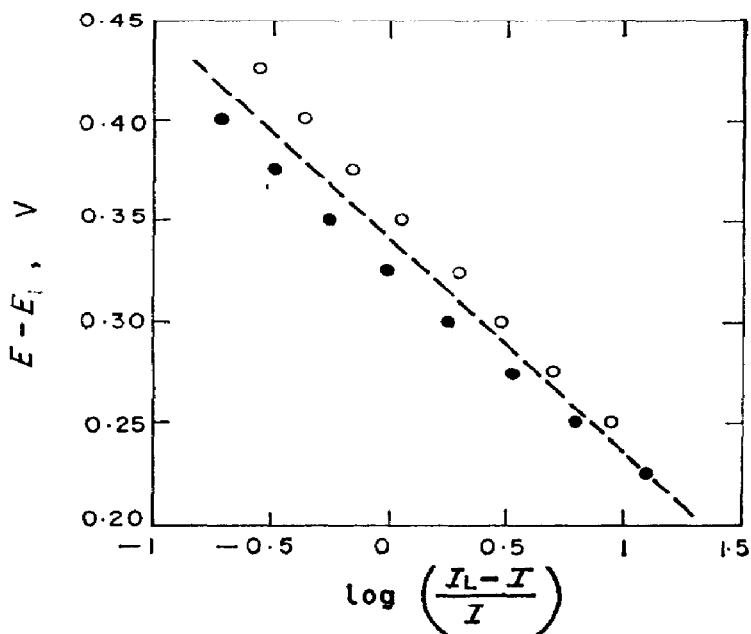


FIG. 8. Plot of $(E - E_1)$ vs $\log\{(I_L)I - I/I\}$ for different cathodic runs. \circ , c_0 , 28.8 mM; 2490 rev/min; 15.5°C; \bullet , c_0 , 44.5 mM; 863 rev/min; 15°C. The slope of the dotted line is $2.3(2RT/F)$.

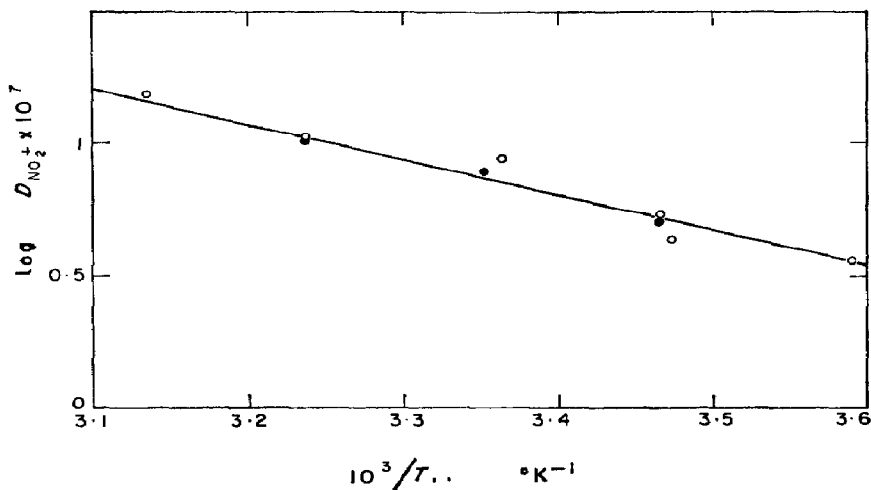


FIG. 9. Arrhenius plot for the diffusion coefficient of NO_2^+ , $c_0 = 9.2$ mM. \bullet , r.d.e.; \circ , cyclic voltammetry.

potential towards the negative potentials, are shown in Figs. 11 and 12. During the negative half-cycle (v negative), there are two well defined current peaks (I and II) and during the positive half-cycle (v positive) there is one clear anodic current peak (III) at the more negative potentials and a smooth cathodic current peak (IV) at ΔE about 0.45 V. There are no drastic changes in the voltogram shape produced by the potential-sweep rate, except the current peak increase and the shift of the potential corresponding to the first cathodic current peak. At the highest sweep rates the double-layer-charging effect is clear at the extremes of the

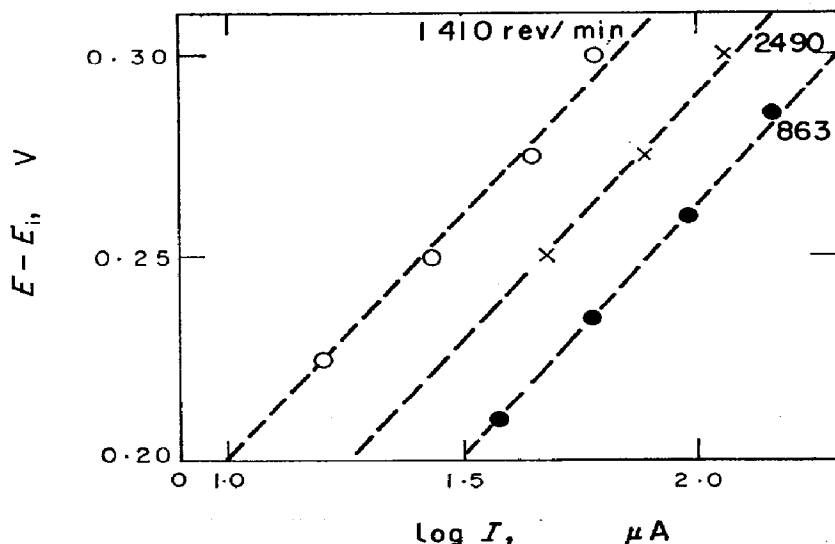


FIG. 10. Tafel plots of the initial portion of cathodic E/I curves. 15.5°C .
 ○, 9.2 mM, 1410 rev/min; ●, 44.5 mM, 863 rev/min; ×, 28.8 mM, 2490 rev/min.
 The slope of the straight lines is 0.116 mV.

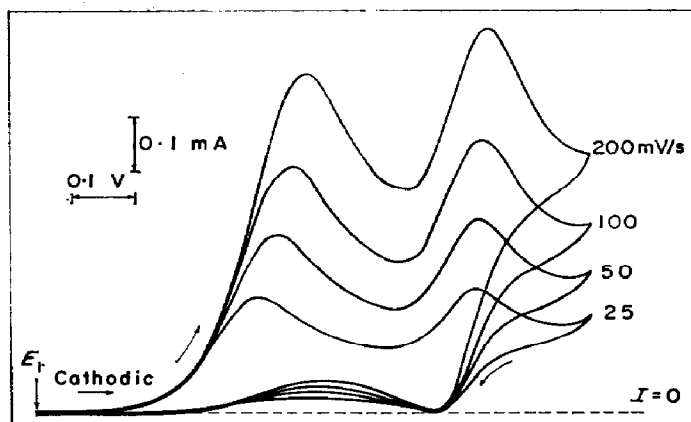


FIG. 11. Cyclic E/I voltammograms at different potential-sweep rates.
 $c_0 = 44.5$ mM; 15.1°C . Electrolyte at rest.

voltammogram (Fig. 12). From the instantaneous current jump when v changes from negative to positive or *vice versa*, the estimated double layer capacitance is $140 \pm 15 \mu\text{F}/\text{cm}^2$. The double-layer correction was made for voltammograms obtained at v larger than 200 mV/s. Figures 13 and 14 exhibit repetitive cyclic E/I voltammograms obtained at two different potential-sweep rates with the electrolyte at rest. It is evident that current peaks I and IV practically disappear after the 6th cycle, while current peaks II and III remain practically unchanged. But if the electrolyte is agitated, so that cyclic voltammetry is combined with the conditions of rotating disk electrode, the repetitive voltammograms, as shown in Fig. 15, appear far different from those already analysed. The first E/I voltammogram starting from E_1 towards the cathodic region presents the current peak I rather higher than those obtained with the successive E/I voltammograms.

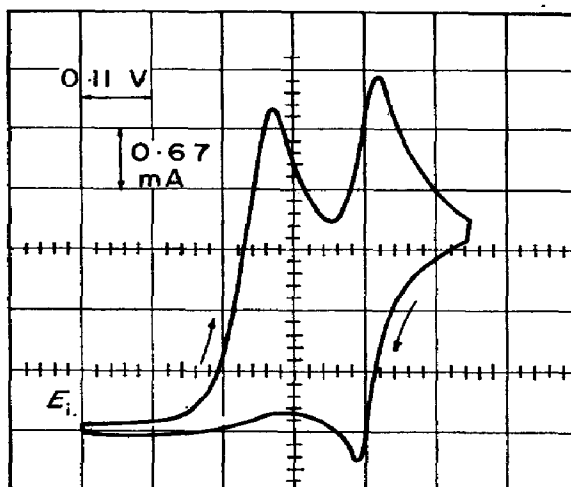


FIG. 12. Cyclic E/I voltogram at 7 V/s.
 c_0 , 56.5 mM; 15°C. Electrolyte at rest.

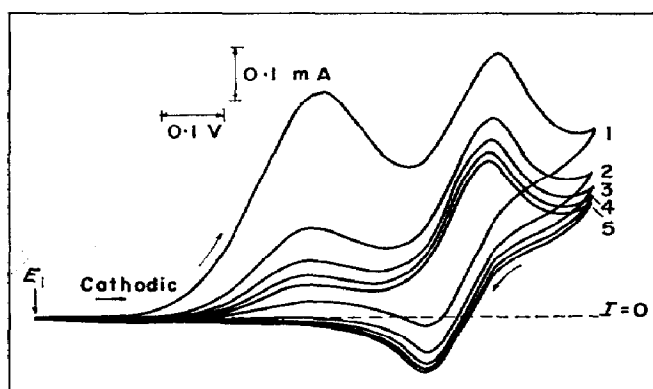


FIG. 13. Five successive cyclic E/I voltograms at $v = 0.1$ V/s.
 c_0 , 44.5 mM; 15°C. Electrolyte at rest.

The potential for this current peak is more positive than that observed in the following voltograms. In the successive cycles this peak is at more negative potentials, as if the electrode reaction requires a higher cathodic overpotential. On the other side, no large changes are observed for peaks II, III and IV in the successive cycles. A common feature of these E/I displays is that the observed currents, including that of the positive half-cycle, are always cathodic, and are larger when a larger rotation speed is employed. Besides, when the rotation speed is increased, peak IV tends to overlap peak I. This suggests that both peaks are related to the same electrode process.

Peak I exhibits a linear dependence of the current peak on the square root of the potential-sweep rate in the whole range of v , c_0 and temperature T , (Fig. 16). The current peak depends linearly on c_0 (Fig. 17).

The current peak II, referred to the $I = 0$ base-line, also follows a linear relationship with the square root of v (Fig. 18). If the current peak is corrected for the base-line

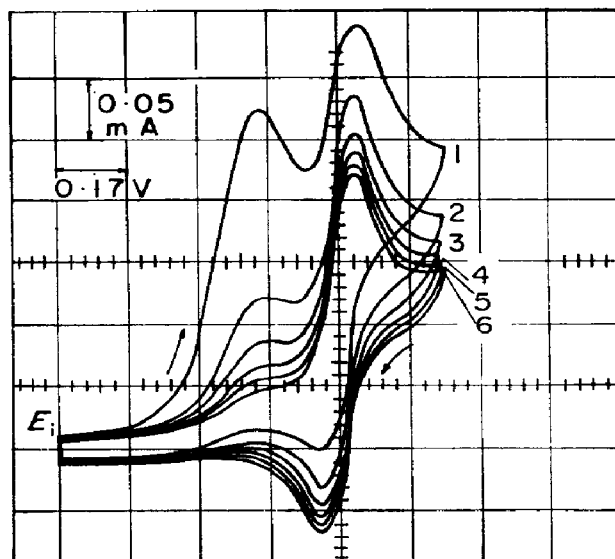


FIG. 14. Six successive cyclic E/I voltammograms at $v = 0.8$ V/s. c_0 , 9.2 mM; 15°C. Electrolyte at rest.

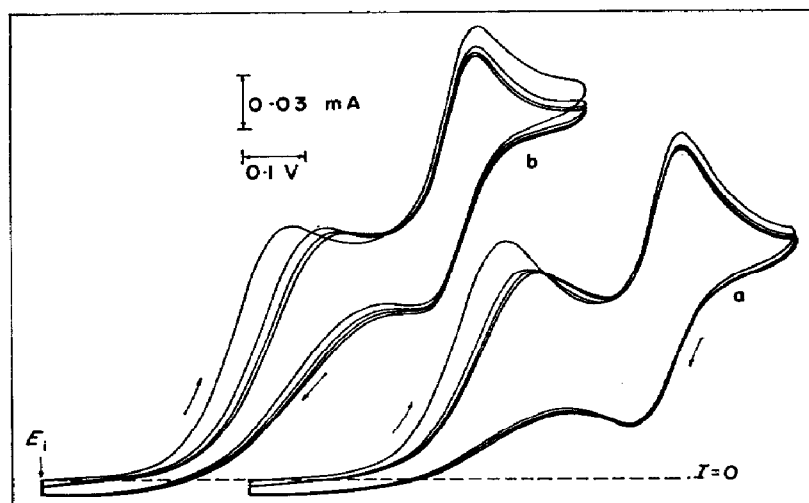


FIG. 15. Four successive cyclic E/I voltammograms at $v = 0.2$ V/s. c_0 , 9.2 mM; 15°C. a, $\omega = 360$ rev/min; b, $\omega = 1130$ rev/min.

of current peak I it also follows the same dependence both on v and c_0 (Figs. 19 and 20). Current peak III is related to current peak II, as deduced from the $(I_p)_{II}/(I_p)_{III}$ ratio. The latter, calculated as described elsewhere,⁸ is practically unity for any v , c_0 and T . The potential $(E_p)_I$, associated with the current peak I, depends linearly on $\log v$ with a slope very close to $2.3(RT/F)$ and it also exhibits a linear $(E_p)_I/\log(I_p)_I$ relationship with a slope very close to $2.3(2RT/F)$ (Fig. 21).

As for the case of the r.d.e., if the E/I curve in the region preceding the current peak I is plotted as a Tafel line (Fig. 22), straight lines are obtained in the whole

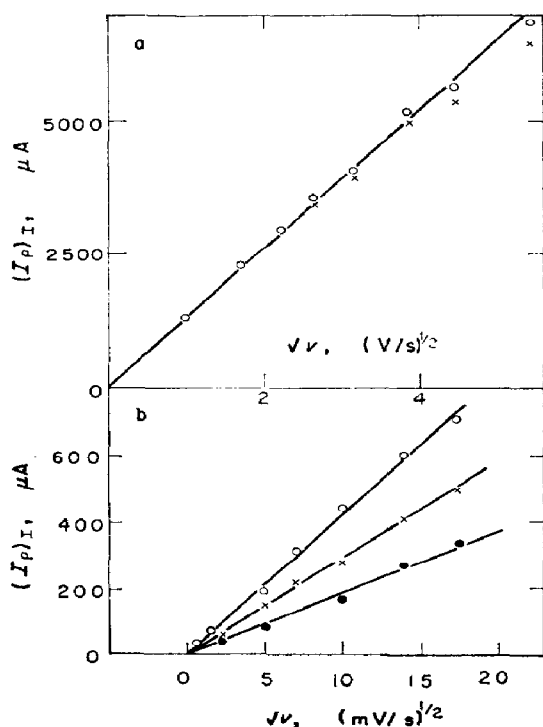


FIG. 16. Dependence of current peak I on the square root of potential sweep rate. a, c_0 , 44.5 mM; 14.3°C. Data corrected for double layer effect. b, \odot , c_0 , 44.5 mM, 15.1°C; \times , c_0 , 28.8 mM 15.5°C; \bullet , c_0 , 19.9 mM, 15.2°C.

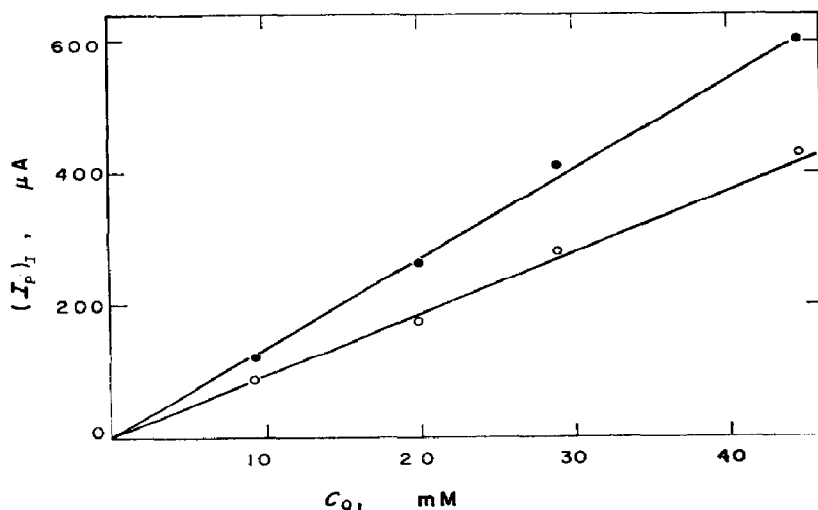


FIG. 17. Dependence of current peak I on NaNO_3 concentration. \bullet , $v = 0.2 \text{ V/s}$; \circ , 0.1 V/s . 15°C.

temperature range investigated, their slopes being practically $2.3(2RT/F)$. The extrapolation of these lines to E_1 gives an arbitrary current at E_1 , which can be used to find the temperature effect on the reaction rate. The current extrapolated at E_1 fits an Arrhenius plot, as seen in Fig. 23, and the experimental activation energy is $13.3 \pm 0.4 \text{ kcal/mole}$.

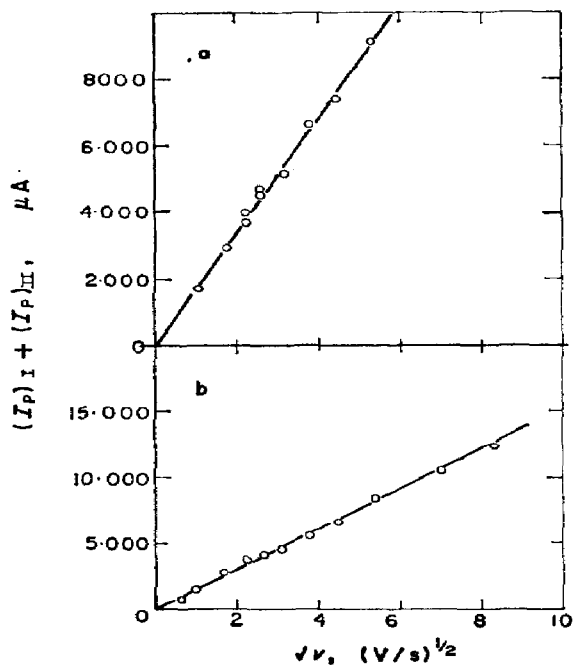


FIG. 18. Dependence of total current peak II on the square root of potential-sweep rate. a, 44.5 mM, 14.8°C; b, 56.5 mM, 5°C.

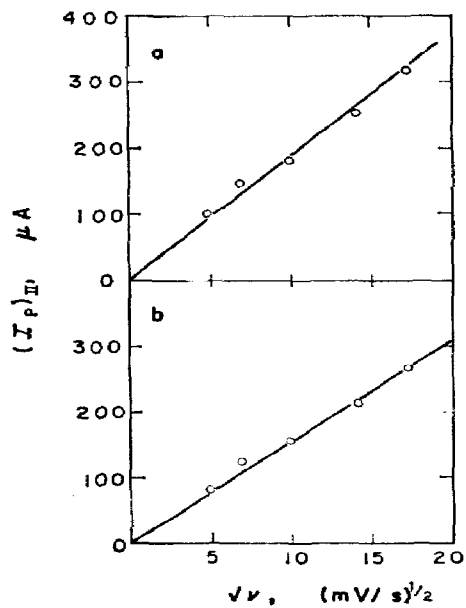


FIG. 19. Dependence of current peak II on the square root of potential-sweep rate. 15.1°C. a, c_0 , 44.5 mM; b, c_0 , 28.8 mM.

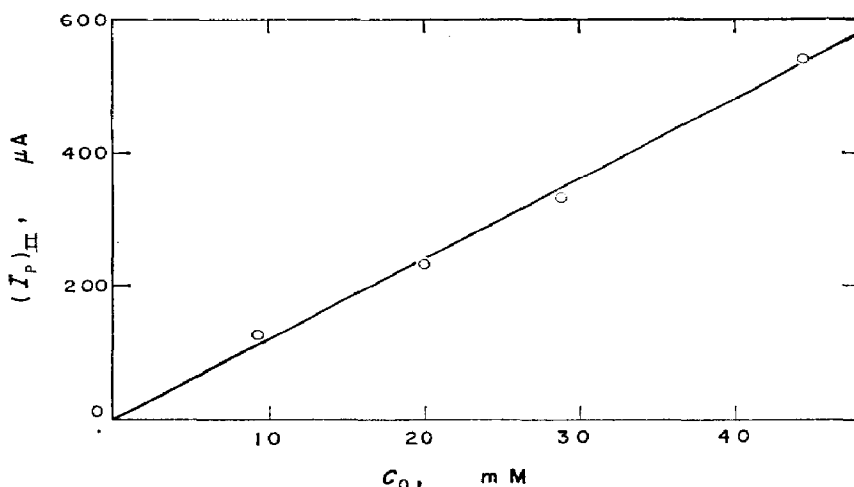


FIG. 20. Dependence of current peak II on NaNO_2 concentration. $v = 0.3 \text{ V/s}$; 15°C .

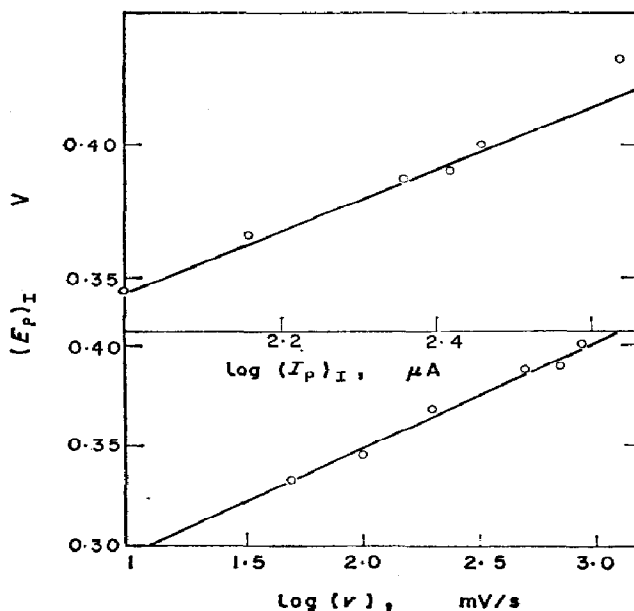


FIG. 21. Semilogarithmic plot of $(E - E_1)$ vs $\log(I_p)_I$ and $\log v$. $c_0, 9.2 \text{ mM}$; 15.5°C .

DISCUSSION

The results clearly show the existence of two electrode processes that occur within definite potential regions and that exhibit different kinetic behaviour. Thus, the process occurring at more positive potentials is markedly more irreversible than the process occurring at less positive potentials. The latter, which is related to current peaks II and III, corresponds to the reversible couple NO^+/NO , which has been recently studied in concentrated sulphuric acid from the kinetic viewpoint.⁴

When NaNO_2 is dissolved in concentrated sulphuric acid the nityl (nitronium)

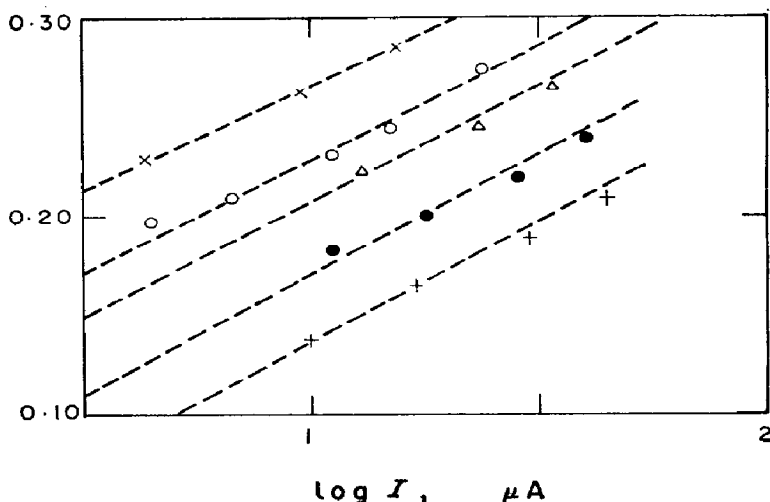


FIG. 22. Tafel plot for the initial region of the E/I voltgrams obtained at different temperatures. \times , 5°C; \circ , 14.8; \triangle , 24.3; \bullet , 35.8; $+$, 46.0; (\times) . c_0 , 9.2 mM. The slope of the straight lines is $2.3(2RT/F)$.

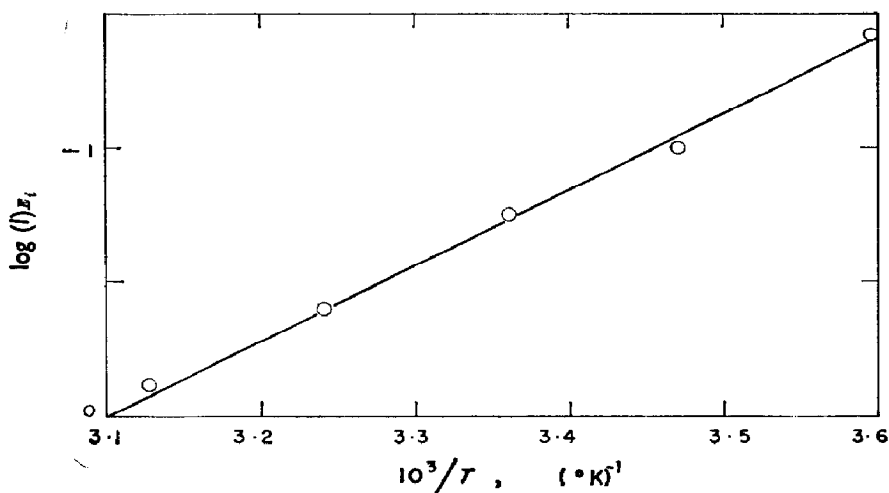


FIG. 23. Arrhenius plot for current extrapolated to E_1 from Fig. 22.

ion is quantitatively formed according to⁶



Therefore in the potential range investigated, the first ion to be electrochemically reduced is NO_2^+ . The reduction of H_3O^+ must take place at potentials more negative than those corresponding to NO^+ reduction in concentrated sulphuric acid.

If NO^+ discharge occurs, and it is not initially present in the solution, its formation must take place as a consequence of NO_2^+ reduction. Therefore, to estimate the concentration of NO^+ that allows its reduction current peak II, we must appeal to kinetic

results obtained for the single reduction of NO^+ dissolved in concentrated sulphuric acid. The E/I cyclic voltogram is given, for NO^+ reduction, by⁹

$$I = nFAc_0 \sqrt{(\pi Da)} \chi(at), \quad (2)$$

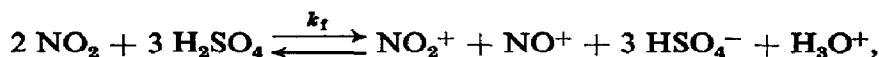
where n is the number of electrons, c_0 the bulk concentration, A the geometrical electrode area, $a = nFv/RT$; and $\chi(at)$ is a function of the applied potential.

The diffusion coefficient of NO^+ at 25°C is $1 \times 10^{-6} \text{ cm}^2/\text{s}$. From (1) the calculated concentration of NO^+ related to current peak II is, Table 1, practically equal to

TABLE 1. CALCULATED NO^+ CONCENTRATIONS. 15.5°C

c_0	c_{NO^+}	c_0/c_{NO^+}
mM	mM	
9.2	10.2	0.902
19.9	18.4	1.08
28.8	26.6	1.08
44.5	44.4	1.00
Mean: 1.015 ± 0.100		

the NaNO_3 concentration. Therefore, we conclude that the reduction of one mole of NO_2^+ yields practically one mole of NO^+ . Furthermore, if NO_2^+ discharge yields NO_2 and the latter dissolves in H_2SO_4 to form NO^+ according to⁶



one would expect a catalytic mechanism to govern the electrode process. If this is the case and k_f is large, then current peak I would be affected, approaching, as $(k_f/v) \rightarrow \infty$, a limiting current, while current peak II would be unaffected. On the other hand, if k_f is small, current peak I would not be affected while current peak II would decrease when v increases.^{9,10}

However, the facts (among others) that the $(I_p)_I/(I_p)_{II}$ ratio is independent of v and in the range of v investigated both current peaks, independently considered, change linearly with $v^{1/2}$, imply that a catalytic mechanism involving reaction (3) is unlikely.

If reaction (3) is excluded, the only possibility of generating quantitatively NO^+ from NO_2^+ is through the formation of NO_2^- as reaction intermediate, the latter undergoing dissolution in the acid yielding NO^+ , which is later reduced to NO , at more negative potentials. Thereby two reaction mechanisms can in principle be postulated to account for the whole cathodic processes.

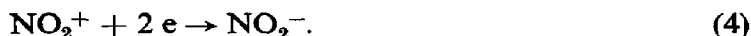
Mechanism I



Mechanism II



Mechanism I comprises a two-electron transfer as primary step followed by a chemical reaction and later a second electron-transfer step. Mechanism II implies a single electron transfer as initial step, yielding NO_2 at the electrochemical interface, which is further reduced to NO_2^- at a rate much faster than that corresponding to its dissolution according to reaction (3). Either reaction Ia in Mechanism I or steps IIa and IIb in Mechanism II occur in the potential region of current peak I. Therefore the over-all reaction associated with it is



Then, two electrons per NO_2^+ act in its reduction on the gold electrode surface. On the other hand, the total process related to current peak II is expressed either by step Ic or IId, known to occur reversibly.⁴ As is known, any chemical reaction between NO and H_2SO_4 is so slow that it does not interfere practically with the existence of the NO/ NO^+ couple when the latter is studied in the time range of voltammetric experiments.

To decide the more likely reaction pathway, let us consider the dependences of the kinetic parameters referred above. If Mechanism I is correct the predictions of an ECE (Electrochemical-Chemical-Electrochemical) mechanism, step Ia being either a reversible or irreversible step, should apply. This however seems not to be the case. It is quite evident that the dependencies of both $(E_p)_I$ on v correspond to an irreversible process and the slopes for the first, (RT/F) , and for the second, $(2RT/F)$, seem to indicate that a one-electron-transfer step is rate-determining under a low degree or surface coverage by reaction intermediates. Therefore on the assumption that we are dealing with an irreversible reaction, and with αn_a , where α is the transfer coefficient assisting the reaction in the cathodic direction and n_a the number of electrons involved up to the rate-determining step, let us calculate $E_p - E_{p/2}$ by means of⁹

$$E_p - E_{p/2} = -1.857 \frac{RT}{\alpha n_a F} \quad (5)$$

where $E_{p/2}$ is the potential at the half current-peak. On applying (5) to current peak I the results shown in Table 2 are obtained. The average αn_a value is 0.49 ± 0.05 .

TABLE 2.

v V/s	E_p V	$E_{p/2}$ V	αn_a
	c_o , 28.8 mM;	15.5°C	
0.025	0.340	0.258	0.556
0.050	0.350	0.270	0.573
0.100	0.373	0.280	0.496
0.200	0.388	0.300	0.524
0.300	0.398	0.307	0.504
			Mean 0.531
	c_o , 44.5 mM;	15.0°C	
1.000	0.433	0.337	0.474
3.000	0.456	0.353	0.449
5.000	0.472	0.367	0.434
7.000	0.489	0.387	0.449
10.000	0.500	0.392	0.426
15.000	0.511	0.406	0.435
			Mean 0.445

Therefore, if α as commonly accepted is taken as 0.5 the number of electrons involved in the rate determining step must be one, and mechanism II, involving the initial discharge reaction as rate-determining, is the more likely.

Consequently, reaction (4) involves two one-electron-transfer steps (IIa and IIb) the first being rate-determining. Then, the equation describing the E/I voltgram is

$$I = nFAc_0 \sqrt{(\pi Db)\chi(bt)}, \quad (6)$$

where $b = \alpha n_a Fv/RT$ and $\chi(bt)$ is the current function for irreversible charge transfer.⁹ This equation implies a linear $(E_{p/2} - E_1)$ vs $\log v$ relationship, which in this case exhibits a slope very close to $2.3(RT/F)$, as seen in Fig. 24.

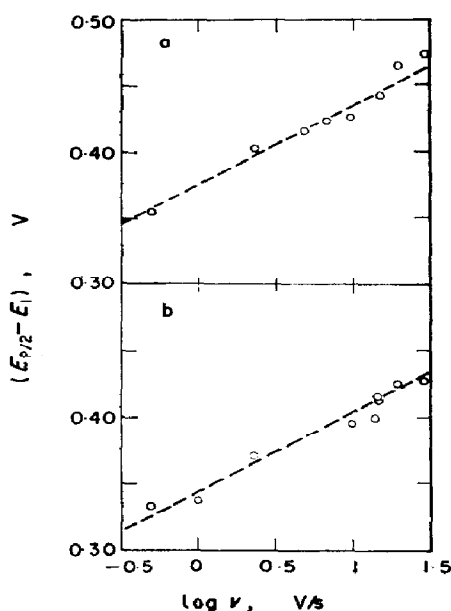


FIG. 24. Plot of $(E_{p/2})_I - E_1$ as a function of $\log v$. c_0 , 56.5 mM. a, 5°C; b, 15°C. Dotted lines correspond to slope $2.3(RT/F)$.

Equation (6) explains the different relationships found between I_p and E_p with v , and between I_p and E_p . Furthermore, as (2) reproduces the shape of the NO^+ reduction voltgram, the preceding conclusion suggests that both equations properly added should reproduce the experimental E/I curves. The excellent agreement between theory and experiment is illustrated in Fig. 25.

We are now in a position to explain the anodic current peak III and cathodic current peak IV. The former is the already known current peak for NO oxidation complementing the NO^+/NO redox couple in concentrated sulphuric acid. Current peak IV is located in the potential region where NO_2^+ reduction occurs. This current peak diminishes when high potential-sweep rates are employed and increases when the rotation speed of the working electrode increases. Hence it is related to the possibility that NO_2^+ is replenished at the electrochemical interface during the duration of the potential sweep. Thus, when the agitation is sufficiently high, current peak IV approaches the shape and location of current peak I.

The reaction sequence discussed before in terms of Mechanism II explains the

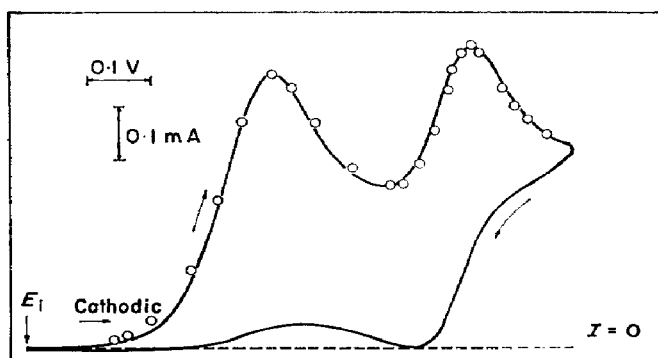


FIG. 25. Experimental single sweep voltammogram and theoretical data (points) calculated from equations (2) and (6).
 c_0 , 28.8 mM; 15.5°C; v , 0.3 V/s; E_i , 0.650 V.

characteristics of the repetitive E/I voltammograms. Once the NO_2^+ which is initially present at the reaction interface has been transformed into NO^+ , the only voltammogram left after various cycles is that corresponding to the NO^+/NO couple, because the latter is a fast electrochemical process. Furthermore as no reversible $\text{NO}_2^+/\text{NO}_2$ or $\text{NO}_2/\text{NO}_2^-$ couple is observed there is no possibility of obtaining NO_2^+ by any backward reaction during the positive half cycle. Therefore, after the first cycle, the reaction interface which was primordially constituted by NO_2^+ as reacting species, is now occupied by NO^+ and NO as reacting entities.

Another evidence for the marked irreversibility of NO_2^+ reduction is found in the rather marked irreproducibility of the E/I curves and their dependence on the history of the gold electrodes. The latter is already verified by comparing the current peak I with those recorded during subsequent cycles, with cyclic voltammetry.

On the basis of (2) and (6) it is possible to evaluate the diffusion coefficient for NO^+ . For the purpose data previously published served for comparison. The result can be compared with the value derived from the rotating disk electrode (Fig. 8). Data are assembled in Table 3 and the different comparisons give a reasonable agree-

TABLE 3. DIFFUSION COEFFICIENTS OF NO_2^+ AND NO^+ -IONS

Temp °C	c_0 mM	$(D_{\text{NO}_2^+}) \times 10^7$ (voltam) cm ² /s	$(D_{\text{NO}_2^+}) \times 10^7$ (rde) cm ² /s	$(D_{\text{NO}^+}) \times 10^7$ (rde) cm ² /s
15.5	9.2	4.34 ± 0.2	4.10 ± 0.2	5.96 ± 0.2
24.3	9.2	6.96	6.43	12.0
35.8	9.2	8.37	8.19	15.2
15.2	19.2	3.63	3.64	5.96
15.1	44.5	3.71	3.86	5.42

ment. D_{NO^+} is always larger than $D_{\text{NO}_2^+}$ indicating that the solvodynamic radius of NO_2^+ is larger than that of NO^+ .

Comparison of mechanism II with other reaction mechanisms

Masek studied the electrochemical reactions of NO_2^+ and NO^+ on the dme under different experimental conditions, arriving at the following reaction scheme.^{1,2}

Mechanism III.

Masek's reaction scheme involves the disproportionation of (NO_2) and obviously in concentrated sulphuric acid, reaction IIIb, yielding NO_2^+ . Therefore the initial product is partially regenerated. It is evident that the mechanism postulated for the reactions on mercury cannot be applied to gold electrodes.

According to Topol, Osteryoung and Christie,³ if the disproportionation reaction in Mechanism III is sufficiently fast, the over-all process would be simply

Mechanism IV.

which is formally analogous to Mechanism I; but the latter has to be abandoned when a detailed kinetic analysis of the first cathodic current peak is made.

Therefore, either there are two mechanisms for the reactions involving NO_2^+ and NO^+ in concentrated sulphuric acid, depending on the nature of the electrode surface, or a common mechanism exists where the nature of the metal influences the concentration of intermediate but produces no marked changes in the mechanism of the reaction. The present work however indicates unambiguously the reaction pathway on gold electrodes for both NO_2^+ and NO^+ reduction in concentrated sulphuric acid.

Acknowledgement—This work is part of the research program of the INIFTA sponsored by the University of La Plata, the Consejo Nacional de Investigaciones Científicas y Técnicas and the Comisión de Investigaciones Científicas de la Provincia de Buenos Aires. C. T. and J. H. thank the Organización de los Estados Americanos (OEA) for the fellowships granted.

REFERENCES

1. J. MASEK, in *Advances in Polarography*, ed. I. S. LANGMUIR, Vol I, p. 340. Pergamon, New York (1960).
2. J. MASEK and H. PRZEWOŁOCKA, *Colln. Czech. chem. Commun.* **28**, 706 (1963).
3. L. E. TOPOL, R. A. OSTERYOUNG and J. H. CHRISTIE, *J. electrochem. Soc.* **112**, 861 (1965).
4. C. TAMAYO, A. J. CALANDRA and A. J. ARVIA, *Electrochim. Acta.* (Accepted for publication.)
5. R. L. EVERY and W. P. BANKS, *Electrochem. Techn.* **4**, 275 (1966).
6. C. K. INGOLD, D. J. MILLEN and H. G. PODE, *J. chem. Soc.* 2576 (1950).
7. G. PAUS, A. J. CALANDRA and A. J. ARVIA, *Anal. Soc. Cient. Arg.*, **192**, 35 (1971).
8. R. S. NICHOLSON, *Analyt. Chem.* **38**, 1406 (1966).
9. R. S. NICHOLSON and I. SHAIN, *Analyt. Chem.* **36**, 706 (1964).
10. J. M. SAVEANT, *Electrochim. Acta* **12**, 753 (1967).